Available online at www.sciencedirect.com
SCIENCE DIRECT
Computational Biology and Chemistry
Computational Biology and Chemistry 29 (2005) 398–411
www.elsevier.com/locate/compbiolchem

A model for short α-neurotoxin bound to nicotinic acetylcholine receptor from *Torpedo californica*: Comparison with long-chain α-neurotoxins and α-conotoxins

D.Yu. Mordvintsev [a,*], Ya.L. Polyak [a], O.V. Levtsova [b], Ye.V. Tourleigh [b], I.E. Kasheverov [a], K.V. Shaitan [b], Yu.N. Utkin [a], V.I. Tsetlin [a]

[a] *Shemyakin-Ovchinnikov Institute of Bioorganic Chemistry RAS, 117997, Miklukho-Maklaya str., 16/10, GSP-7, Moscow, Russia*
[b] *M.V. Lomonosov Moscow State University, Biology Faculty, Department of Biophysics, 111992, Leninskie Gory, 1, Moscow, Russia*

Received 14 August 2005; received in revised form 14 August 2005; accepted 15 September 2005

Abstract

Short-chain α-neurotoxins from snakes are highly selective antagonists of the muscle-type nicotinic acetylcholine receptors (nAChR). Although their spatial structures are known and abundant information on topology of binding to nAChR is obtained by labeling and mutagenesis studies, the accurate structure of the complex is not yet known. Here, we present a model for a short α-neurotoxin, neurotoxin II from *Naja oxiana* (NTII), bound to *Torpedo californica* nAChR. It was built by comparative modeling, docking and molecular dynamics using ^{1}H NMR structure of NTII, cross-linking and mutagenesis data, cryoelectron microscopy structure of *Torpedo marmorata* nAChR [Unwin, N., 2005. Refined structure of the nicotinic acetylcholine receptor at 4 Å resolution. J. Mol. Biol. 346, 967–989] and X-ray structures of acetylcholine-binding protein (AChBP) with agonists [Celie, P.H., van Rossum-Fikkert, S.E., van Dijk, W.J., Brejc, K., Smit, A.B., Sixma, T.K., 2004. Nicotine and carbamylcholine binding to nicotinic acetylcholine receptors as studied in AChBP crystal structures. Neuron 41 (6), 907–914] and antagonists: α-cobratoxin, a long-chain α-neurotoxin [Bourne, Y., Talley, T.T., Hansen, S.B., Taylor, P., Marchot, P., 2005. Crystal structure of Cbtx–AChBP complex reveals essential interactions between snake alpha-neurotoxins and nicotinic receptors. EMBO J. 24 (8), 1512–1522] and α-conotoxin [Celie, P.H., Kasheverov, I.E., Mordvintsev, D.Y., Hogg, R.C., van Nierop, P., van Elk, R., van Rossum-Fikkert, S.E., Zhmak, M.N., Bertrand, D., Tsetlin, V., Sixma, T.K., Smit, A.B., 2005. Crystal structure of nicotinic acetylcholine receptor homolog AChBP in complex with an alpha-conotoxin PnIA variant. Nat. Struct. Mol. Biol. 12 (7), 582–588]. In complex with the receptor, NTII was located at about 30 Å from the membrane surface, the tip of its loop II plunges into the ligand-binding pocket between the α/γ or α/δ nAChR subunits, while the loops I and III contact nAChR by their tips only in a 'surface-touch' manner. The toxin structure undergoes some changes during the final complex formation (for 1.45 rmsd in 15–25 ps according to AMBER'99 molecular dynamics simulation), which correlates with NMR data. The data on the mobility and accessibility of spin- and fluorescence labels in free and bound NTII were used in MD simulations. The binding process is dependent on spontaneous outward movement of the C-loop earlier found in the AChBP complexes with α-cobratoxin and α-conotoxin. Among common features in binding of short- and long α-neurotoxins is the rearrangement of aromatic residues in the binding pocket not observed for α-conotoxin binding. Being in general very similar, the binding modes of short- and long α-neurotoxins differ in the ways of loop II entry into nAChR.

Keywords: Snake three-fingered short α-neurotoxin; Nicotinic acetylcholine receptor; Toxin–receptor complex; Experimental data based model

1. Introduction

Short- and long-chain α-neurotoxins from snake venoms are potent blockers of nicotinic acetylcholine receptors (nAChR) (see reviews Nirthanan and Gwee, 2004; Tsetlin, 1999; Tsetlin and Hucho, 2004). Short α-neurotoxins consist of 60–62 amino acid residues and include four disulfide bridges, whereas long α-neurotoxins have 66–75 residues and five disulfides. The spatial structure of these toxins is built by three loops I–III ("fingers", Fig. 1d) confined by four disulfide bridges, whereas the fifth disulfide bond of long α-neurotoxins is situated close to the tip of the central loop II. This spatial structure known as a "three-finger fold" is characteristic for different proteins (α-neurotoxins, cytotoxins, muscarinic toxins, acetylcholine

Abbreviations: nAChR, nicotinic acetylcholine receptors; AChBP, acetylcholine-binding protein; MD, molecular dynamics; NTII, α-neurotoxin II

* Corresponding author. Tel.: +7 095 330 7374; fax: +7 095 335 5733.
E-mail address: chlorine@yandex.ru (D.Yu. Mordvintsev).

1476-9271/$ – see front matter © 2005 Elsevier Ltd. All rights reserved.
doi:10.1016/j.compbiolchem.2005.08.007

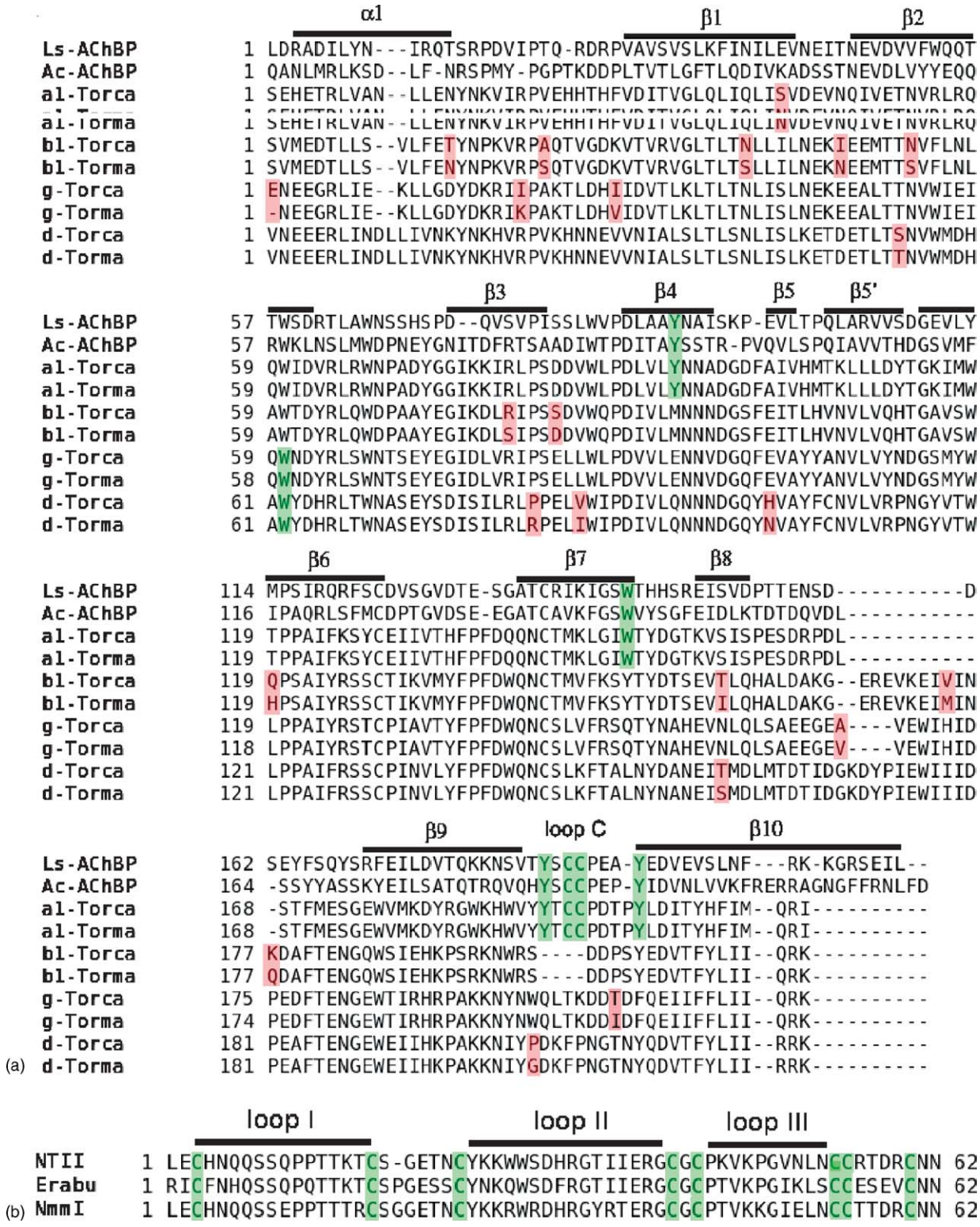

Fig. 1. (a) Alignment of nAChRs subunits from *Torpedo californica* (Torca), *Torpedo marmorata* (Torma), AChBPs from *Aplysia californica* (Ac) and *Lymnaea stagnalis* (Ls) according to the LGIC database. α-, β-, γ-, δ-Subunits of nAChR are marked as a1, b1, g and d, respectively. Substitutions in nAChR subunit sequences of *Torpedo californica* and *Torpedo marmorata* are shown in pink. Aromatic residues and vicinal cysteines of the C-loop critical for acetylcholine binding are shown in lime. Secondary structure elements are marked with the bars. (b) Alignment of snake short α-neurotoxins–neurotoxin II from *Naja oxiana* (NTII), erabutoxin a from *Laticauda semifasciata* (Erabu) and neurotoxin I from *Naja mossambica mossambica* (NmmI). Cysteines are shown in lime and loops are marked with the bars. The structural nomenclature often used for AChBP or the extracellular domain of nAChR (c), loop between β3 and β4 usually designated as A is not marked), and for the short-chain α-neurotoxins (d). One protomer of *Lymnaea stagnalis* AChBP (1UX6) from side view and NMR structure of NTII (1NOR) from "concave side" are presented. All figures were done with PyMOL 0.97 (www.pymol.org). (For interpretation of the references to color in this figure legend, the reader is referred to the web version of the article.)

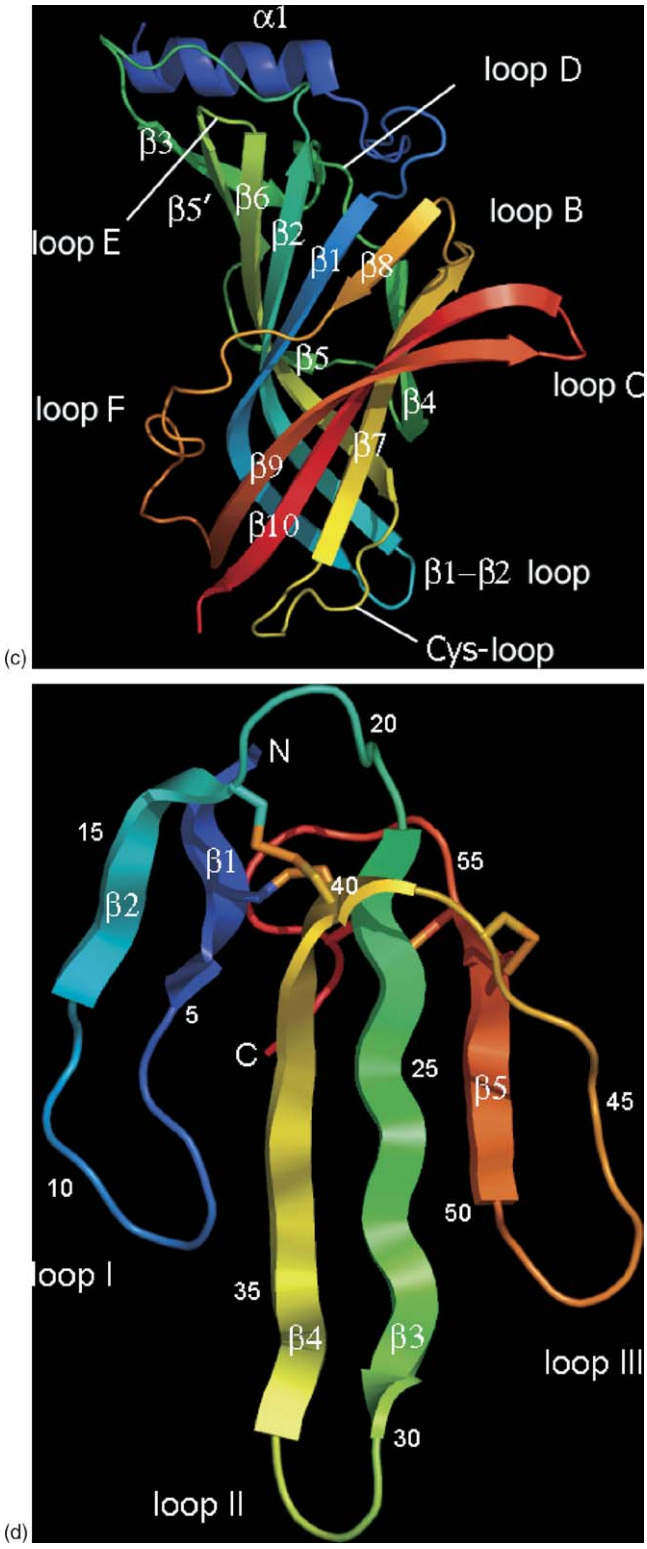

Fig. 1. (*Continued*).

esterase inhibitors and some other) from snake venoms (Tsetlin, 1999). α-Neurotoxins are currently used in pharmacological studies of diverse nAChRs. An accurate knowledge of the mode of α-neurotoxin–nAChR interaction is not only of great fundamental importance for understanding protein–protein recognition, but also as a way for rational design of new nAChR agonists and antagonists for medical purposes.

A possibility to visualize the detailed spatial models of the toxin–nAChR complexes has appeared only recently. It took almost 25 years to come from the first electron microscopy structure *Torpedo marmorata* nAChR (Stroud et al., 1990), which gave an idea of general form and dimensions of the protein, to the 4 Å resolution cryo-electron microscopy structure of this receptor (Unwin, 2005). The structural studies have been focused for many years on the nAChR from the electric ray of *Torpedo* species, since this was the only nAChR, which could be obtained in preparative amounts. During this period, X-ray and NMR-structures have been solved for numerous short and long α-neurotoxins (see reviews Nirthanan and Gwee, 2004; Tsetlin, 1999; Tsetlin and Hucho, 2004 and the respective structures in PDB). However, no structure of the α-neurotoxin–nAChR complex is available although the cocrystals of fluorescence-labeled α-bungarotoxin, and *Torpedo* nAChR have been recently described (Paas et al., 2003). Therefore, ideas on the topography of the toxin–nAChR complexes were based until recently on less direct methods including analysis of nAChR interactions with selectively labeled α-neurotoxins (bearing spectroscopic, photoaffinity or other labels) and mutations in toxins, nAChR or in both of them (pair-wise mutation analysis). Until high-resolution structure became available for the *Torpedo* extracellular domain (where α-neurotoxins, as well as other cholinergic ligands are known to bind) (Unwin, 2005), all those biochemistry and molecular biology data could lead to only very rough models.

The situation changed dramatically when a high-resolution X-ray structure of the acetylcholine-binding protein (AChBP) from mollusk *Lymnaea stagnalis* was solved (Brejc et al., 2001; Celie et al., 2004). This water-soluble protein is an excellent model for the extracellular domains of diverse nAChRs. Since it has a high affinity for long α-neurotoxins, the models were first proposed for AChBP or nAChR complexes with α-cobratoxin or α-bungarotoxin (Fruchart-Gaillard et al., 2002; Harel et al., 2001; Samson et al., 2002). Recently, the crystal structure has been solved for AChBP complex with α-cobratoxin (Bourne et al., 2005). However, there were no "Angström-resolution" models for complexes of short-chain α-neurotoxins, which bind only to muscle and *Torpedo* nAChR, contrary to the long α-neurotoxins able to bind with neuronal α7 nAChR as well.

Here, we report the model of the *Torpedo californica* nAChR extracellular domain complexed to a short-chain α-neurotoxin II (NTII) from the *Naja oxiana* cobra venom. The basis of this model is a set of ^{1}H NMR structures for NTII (Golovanov et al., 1993, 1NOR, accession number by Protein Data Bank) and a wealth of labeling and mutagenesis data available for this and other homologous short α-neurotoxins. When building the model of *T. californica* nAChR extracellular domain, not only the cryoelectron microscopy data for the *T. marmorata* receptor (free of any ligands, 2BG9) (Unwin, 2005) were taken into account, but also the data for AChBP complexes with agonists (1UX6 and 1UW6) and α-conotoxin (2BR8) (α-conotoxins, neurotoxic peptides, are potent and selective antagonists of

nAChR). A comparison of the results obtained with the recently published 4 Å X-ray structure of the AChBP complex with α-cobratoxin (Bourne et al., 2005) revealed common features in binding of the short- and long α-neurotoxins, but also shed light on some differences in their binding modes.

2. Experimental

2.1. Model building

All models of the extracellular domains of the *T. californica* nAChR subunits were constructed using the program MODELLER 7v7 (http://www.salilab.org/modeller) with the sequence alignment from LGIC database (http://www.ebi.ac.uk/compneur-srv/LGICdb/LGICdb.php, see Fig. 1). The experimental structures were from Protein Data Bank (http://www.rcsb.org/pdb). Multiple requests to the Swiss-Model server (http://swissmodel.expasy.org) were used as control in several cases. The structure verification was carried out with WHAT_CHECK program (http://swift.cmbi.nl/gv/whatcheck/), after which the structures were relaxed (300 steps of steepest descent with cut-off 10 Å) with GROMOS'96 instruments included into the SPDBViewer 3.7 sp5 (http://swissmodel.expasy.org/spdbv/).

Every subunit was constructed separately and independently from others. β-Subunit was created with only β-subunit of *T. marmorata* nAChR (B-chain of 2BG9, 11 amino acid substitutions) as template because no structural changes were expected to be evoked by the toxin binding. For γ- (additional N-terminal residue and four amino acid substitutions as compared to *T. marmorata*) and δ- (six amino acid substitutions) subunits, the templates of the α1-helix, β4, β5 and β7 sheets, loops A, C and D (see Fig. 1c for nomenclature) were from 2BG9 chains E and C, respectively. The β1, β2, β3, β5′, β6, β8, β9 and β10 sheets, loops E and F were modeled on the basis of the structures of *L. stagnalis* AChBP complexes with nicotine (1UW6) and carbamylcholine (1UV6), as well as the X-ray structure of the complex of *Aplysia californica* AChBP with conotoxin [A10L,D14K]PnIA (2BR8). The results of Bourne et al. (2005), which became available after our model was built, were used during the analysis of the model and its refinement. α-Subunit (one amino acid substitution) was constructed in four variants, designated as V1–V4. For variant V1, the A- and D-chains of 2BG9 structure were used as unique templates to construct the extracellular domain of the *T. californica* nAChR, with virtually closed entrance to the channel free of ligand. Model V2 was constructed as V1, but the C-loop was displaced outward from the body of the receptor with the same shift angle of the C-loop as was observed in 2BR8. The general structure of the loop was not changed, and the relative position of the Cys192–Cys193 disulfide was conserved. The third variant (V3) was analogous to V2, but the β4, β5 and β7 sheets, the beginning of the β2, loops A, B and D were modeled using the 2BR8, 1UW6 and 1UV6 structures. Thus, the binding pocket was rebuilt in the same way as found for AChBP complexes with carbamylcholine, nicotine or α-conotoxin (virtually the same rearrangement as in case of bound low molecular weight ligands, except for the position of the C-loop), but the position of the C-loop was different from that in AChBP complexes. This C-loop position was changed in the variant V4 of the α-subunit model, which was similar to V3 but with C-loop and β9–β10 hairpin constructed on the base of 2BR8 structure.

The subunits were assembled into pentamers using rotational angles from 2BG9 for β, γ and δ-subunits. For α-subunit position, the angle was also from 2BG9 in one case and from AChBP–conotoxin structure in another. After construction all models were minimized using GROMOS'96 instruments as was also done after single subunit modeling. Thus, 16 different structures of the pentameric form of the extracellular domain of the *T. californica* nAChR were created.

2.2. Docking simulations and solutions selection

The NMR structure of NTII from *N. oxiana* (1NOR, 19 solutions) was used for docking studies. 3D modeling of the spin- and photoactivatable labels attached to NTII and assessment of their mobility was performed with Chem3D Pro 9.0 software (CambridgeSoft) and TINKER program (http://dasher.wustl.edu/tinker/), both using MM2 force field (Burkert and Allinger, 1982).

Preliminary approximate docking simulations were performed under HEX 4.2b (http://www.csd.abdn.ac.uk/hex/) for all models built. All 19 NMR structures were docked to 16 models of nAChR extracellular domain. Thus, this flexible ligand was docked to the rigid receptor wherein only the C-loop and binding pocket residues were flexible. Final refined solutions were obtained with HADDOCK 1.3 (http://www.nmr.chem.uu.nl/haddock/). As HADDOCK allows managing the simulation by some biochemical information, the data on photoaffinity labeling with azidobenzoyl derivatives of NTII with photogroups at Lys26, Lys44 and Lys46 were used (Kreienkamp et al., 1992; Tsetlin et al., 1982). Subsequent visual analysis in the SPDBViewer allowed us to reject false positive solutions: those positions of the toxin in the binding pocket proposed by the program were discarded which were not at least in rough accordance with the available data on chemical modification and mutagenesis of homologous short neurotoxins. Molecular dynamics procedures were run over the solutions considered valid after this selection.

2.3. Molecular dynamics (MD)

Further refinement of the constructed model was done on the basis of MD simulations. The runs were done for the system comprising α and γ-subunits and the toxin disposed according to the docking simulations.

For the purpose of comparison, two independent methods were applied: Langevin dynamics GROMACS 3.2.4 package (http://www.gromacs.org/) with GROMOS'87 force field (Gunsteren and Mark, 1992) and molecular dynamics PUMA package (Lemak and Balabaev, 1996) with AMBER'99 force field (Wang et al., 2000). Rather short (100 ps) trajectories were calculated at the temperature 300 K, dielectric permittivity $\varepsilon = 1$. Time step of integration procedures was taken as small as 1 fs.

Radius of truncation for Coulomb interactions was 20 Å. No periodic boundaries were applied.

For the first force field the following parameters were set. Friction coefficient was of 1000 amu/ps, Lennard–Jones interactions were cut off at 20 Å without shift or switch functions. Within the second force field Lennard–Jones interactions were calculated only up to 16 Å (at that, from 15 to 16 Å a polynomial switch function was applied). We applied collisional thermostat (Lemak and Balabaev, 1995). Unlike Berendsen or Nosé–Hoover thermostats, it does not lead to physically incorrect dynamic behavior of the system (Golo and Shaitan, 2002; Golo et al., 2004).

3. Results and discussion

3.1. Conformational properties of NTII and its labeled derivatives

NTII from *N. oxiana* cobra venom (Fig. 1b and d) was chosen for building a model of the *Torpedo* nAChR complex with a short neurotoxin because numerous studies on this particular toxin have been earlier performed (see references in reviews Hucho et al., 1996; Tsetlin, 1999; Tsetlin and Hucho, 2004). These included its NMR, and optical spectroscopy studies, preparation of spin-labeled, fluorescent and photoactivatable derivatives as well as analysis of their interaction with the *Torpedo* receptor. The literature also contains abundant information on similarly modified homologous short neurotoxins and their mutant forms (see review Servent and Menez, 2001). Thus, at our disposal was quite impressive amount of data, which might be used to control the model creation at every step.

The photolabeling data were used as managing criterion of the docking. The flexibility of the whole molecule and of the lysine side chains with or without grafted labels was assessed for more accurate solution filtration. As a final step, positive solutions were submitted for MD simulations and analyzed using the data on labeling and mutagenesis of homologous toxins.

The mobility of photoactivatable labels (in most cases azidobenzoyl ones) introduced at the N-terminus or lysine residues of the NTII was estimated by computational methods and compared with the experimentally measured mobility of spin and fluorescent labels at the same positions (Ivanov et al., 1980; Timofeev and Tsetlin, 1983; Tsetlin et al., 1979a). In addition, to characterize the mobility of the lysine side chains the NMR data for NTII and homologous toxin α from *Naja nigricollis* and erabutoxin b from *Laticauda semifasciata* were also used (Arseniev et al., 1981; Guenneugues et al., 1997). In a good accordance with these experimental results our modeling showed that the labels on Lys44 and Lys46 were the most flexible, on Leu1 and Lys15, somewhat less. Those on Lys26 and especially on Lys25 were limited in their fluctuation by the adjacent side chains. The labels on Lys15, Lys44 and Lys46 were found to be noticeably exposed, in contrast to those on Lys25 and Lys26, which agrees with the measured accessibility of the respectively positioned spin labels to paramagnetic probes (Tsetlin et al., 1982).

The structure of NTII was previously shown to be very stable and the incorporation of labels had practically no effect on the general fold of the toxin over a wide range of pH and temperature, the most marked change being observed when the Lys25 was labeled (Arseniev et al., 1981; Khechinashvili and Tsetlin, 1984; Tsetlin et al., 1979b). According to our calculations, the Lys25-modified toxin exhibited already at room temperature a mobility of polypeptide chain of loops I and II similar to that of the wild-type toxin at 80–85 °C. Thus, we came to conclusion that grafting of azidobenzoyl labels should not critically affect both the toxin structure and its binding mode to the receptor. This conclusion is also supported by the relatively high activity of different acylated derivatives of short neurotoxins (Blinov et al., 1982; Chicheportiche et al., 1972; Hori and Tamiya, 1976; Yang, 1974). Interestingly, the drop in the activity was bigger if a larger label was introduced. Therefore, we considered justified to use these NMR and CD data for preliminary quantification of the flexibility of unbound toxin and to apply information from cross-linking experiments on NTII azidobenzoyl derivatives as managing standards in HADDOCK simulations.

3.2. Building a model for the T. californica nAChR extracellular domain and preliminary docking of NTII

We decided to construct the extracellular domain of *T. californica* nAChR taking into account a large body of experimental data on NTII binding to this receptor. All its subunits are highly homologous to the corresponding subunits of the *T. marmorata* nAChR (Fig. 1a), whose 4 Å resolution cryo-electron microscopy structure was recently solved (Unwin, 2005), and were satisfactorily modeled. The only exception is the δ-subunit 168–177 fragment not resolved in the *T. marmorata* structure and structurally too different from the respective fragment of AChBP for precise comparative modeling. For this reason, docking simulations were carried out on the α–γ interface and then the results were fitted to α–δ interface with structural alignment of the δ-subunit CA-atoms (C^{α}-atoms of amino acid residues in PDB nomenclature) on the γ-chain. This is acceptable approximation because NTII (a short-type α-neurotoxin) was shown not to distinguish these two binding sites (Tsetlin et al., 1979a). On the contrary, several low-molecular weight ligands and many α-conotoxins have different affinities to these binding sites (Hucho et al., 1996; Neubig and Cohen, 1979; Utkin et al., 1994). To complete the pentameric extracellular domain, β-subunit possessing only a structural role in the muscle-type nAChR (Changeux and Edelstein, 1998; Stroud et al., 1990) was built.

The model of the pentameric domain (both of *T. californica* and *T. marmorata*) built using 2BG9 structure (model V1, see Section 2) as a template could not generate any stable solution for the complex with the toxin. Neither V2 nor V3 variants could adopt any position of the NTII correlating with photoaffinity labeling, and the respective solutions have been totally rejected as false. As a result only the V4 model was successfully used for docking simulations both in HEX and HADDOCK. Interestingly, a proper solution could not be obtained if the rotational angle of the 2BG9 structure was used. In this case the relative subunit position was determined by fitting on two adjacent protomers of 2BR8. The orientation and packing inconvenience were later eliminated by molecular dynamics. The overall struc-

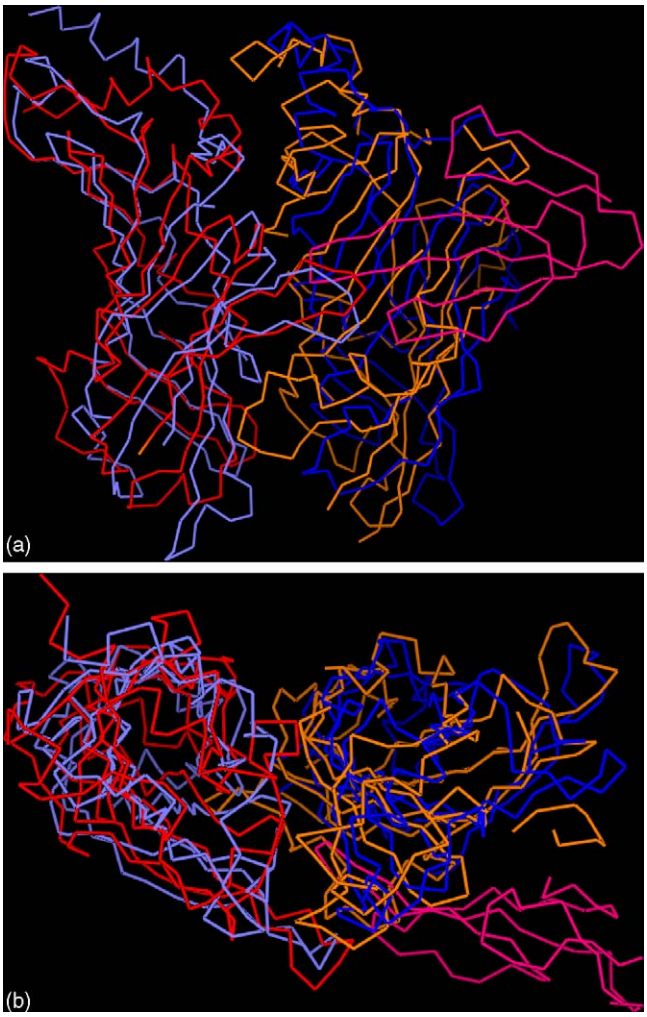

Fig. 2. Fit of nAChR α–γ interface with no ligand bound (by 2BG9, α-subunit in slate, γ-subunit in blue) and with NTII bound (α-subunit in red, γ-subunit in orange, toxin in hot pink) represented from side view (a) and top (b). Relative position of subunits in pentamer is retained. (For interpretation of the references to color in this figure legend, the reader is referred to the web version of the article.)

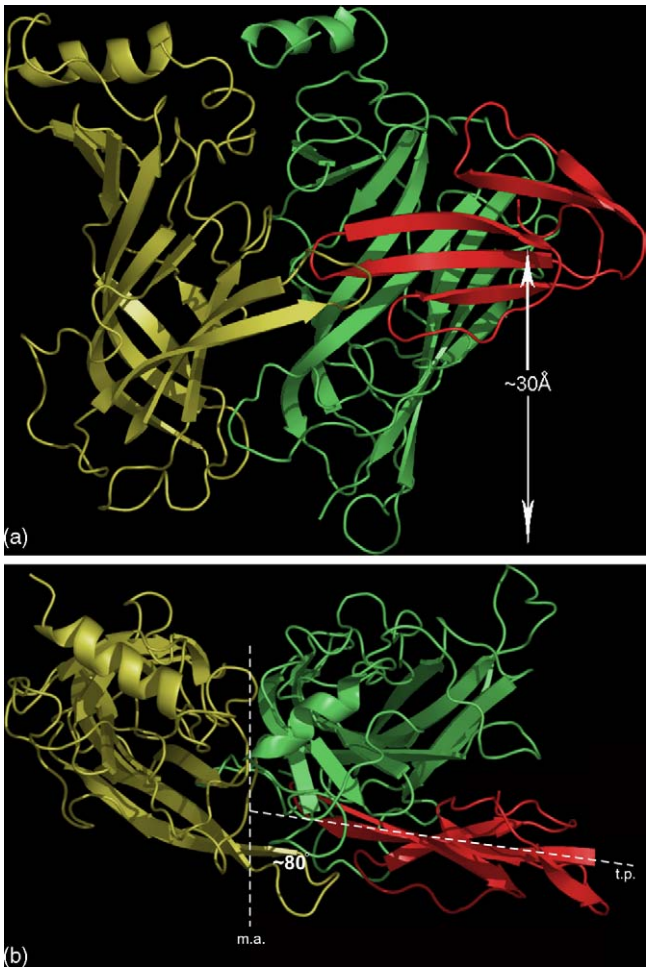

Fig. 3. Overall view of the model refined with MD simulation from side (a) and top (b) for α–γ subunit interface in complex with NTII. The rotational angle of subunits is equal to that in pentameric nAChR. Distance to the virtual membrane outer surface as well as the angles between the toxin plane (t.p.) and median axis (m.a.) is shown. Designation by color: α-subunit in yellow, γ-subunit in green, NTII in red. (For interpretation of the references to color in this figure legend, the reader is referred to the web version of the article.)

ture of final complex was found to be similar to 2BG9, but the rotational angle of the α-subunit still was different from that observed for the intact receptor (Unwin, 2005). We concluded that there should be a 5–6° rotation of the α-subunit extracellular domain to allow the toxin to reach the binding pocket (Fig. 2). This value is smaller than the 10–15° turn of the α-subunit postulated as necessary for agonist binding (Unwin, 2005; Unwin et al., 2002).

3.3. Refinement of the model and comparison with experimental data for short α-neurotoxins

According to our model, NTII in complex with the nAChR is situated at about 30 Å from the membrane surface (Fig. 3). Its molecular axis, defined by the direction of the β3-sheet (see Fig. 3), lies at an ∼80° angle relative to the median axis and at a small angle to the cylinder wall, practically perpendicular to the membrane surface (Fig. 3b). About one third of the toxin loop II is plunged into the ligand-binding pocket, located at the interface between two nAChR subunits, while the loops I and III contact the receptor residues by their tips only (Fig. 3, Tables 1 and 2). The "concave side" of the loops II and loop III is very close to the protruding C-loop of the α-subunit of the receptor, while the loop I, N-terminus and "convex side" of the loop III are accessible to the solvent. The loop III is also contacting the F-loop of the adjacent subunit. In general, disposition of NTII in the model is in good agreement with a study of a homologous α-toxin from *N. nigricollis* (Teixeira-Clerc et al., 2002). These authors showed that the loop II of the receptor-bound toxin is hidden and not accessible for streptavidin, while the loop I and "convex side" of the loop III are exposed to the solvent. The penetration of the loop II into the binding pocket easily explains this fact. It has also been predicted that the toxin should lie at ∼90° angle to the membrane surface, the loop III being the closest to it. The same disposition is clearly observed in our model, built on the basis of different data.

Table 1
Amino acid residues, participating in interactions of NTII with receptor (α–γ interface) determined by docking simulation

NTII	nAChR subunit interface	
	Principal side	Complementary side
Loop I		
Ser 9		Asp113, Ser115, Tyr111
Gln 10		Asp113, Ser115
Loop II		
Trp 28	Cys193	
Ser 29		Glu57
Asp 30	Cys192–Cys193	Tyr117(O-OH)
His 31		Tyr198, Tyr190
Arg 32	***Trp149*** Trp149(NH1/2, NE2-O) Thr74(NE2-OG)	Leu109, Asn107, Tyr117
Gly33		Tyr117, Gln59
Thr34		Glu 57,Gln59(OG-NE2)
Loop III		
Lys 46	Thr191	
Pro 47		Glu166
Gly 48		Ile171
Asn 50		Ser161, (Lys34)

The types of interactions are shown with different fonts: simple, van-der-Waals; underlined, H-bond (toxin residue atom-receptor residue atom); bold italic, pi-cation; in brackets, doubtful or very weak.

Table 2
Amino acid residues, participating in interactions of NTII with receptor (α–γ interface) after 100 ps molecular dynamics simulation (AMBER'99 force field)

NTII	nAChR subunit interface	
	Principal side	Complementary side
Loop I		
His4		**Asp26**
Gln7		(Asn112), (Tyr111)
Ser8		Asn61(OG-ND), Asp113, Ser115
Ser9		Lys23(OG-NZ), Asn61, Asp113
Gln10		Asn60, Asp61
Loop II		
Lys25		**Asp30**, Asn157, Gln159(NZ-OE1)
Trp27		Ser161
Trp28	Cys192–Cys193	
Ser29		Lys34(OG-NZ)
Asp30	Tyr198(OD1/2-OH), Tyr190	Lys34(O-NZ), **Arg79**, Tyr117(O-OH)
His31	Tyr93	Trp55
Arg32	***Trp149***	Asn107(NE1-O)
Gly33		Tyr117, Glu57
Thr34		Gln59
Arg38		**Asp30**
Loop III		
Lys44		Ala167(NZ-O)
Lys46	Thr191(NZ-OG,O)	(***Trp170***)
Pro47		Ala167
Asn50		Glu164(ND2-OE1)
Asn52		Glu163(ND2-O)
Asn61		Asn157(OD1-ND2)

The types of interactions are shown with different fonts: simple, van-der-Waals; underlined, H-bond (toxin residue atom-receptor residue atom); bold, ionic pair; bold italic, pi-cation; in brackets, doubtful or very weak.

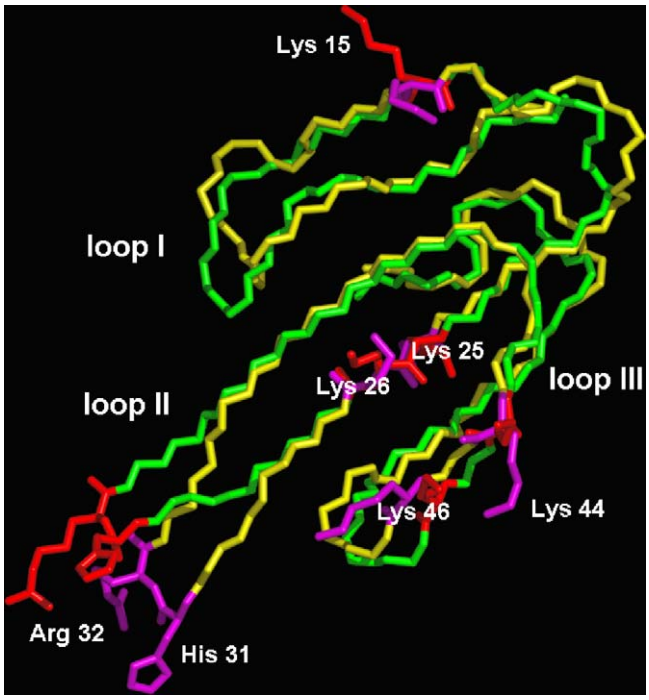

Fig. 4. NMR structure of NTII (green) in solution (1NOR) and its structure in binding pocket of nAChR (yellow) generated by MD fitting. Side chains of lysines, His31 and Arg32 are marked in red for NMR, in magenta for MD. All lysine residues and loops are shown. (For interpretation of the references to color in this figure legend, the reader is referred to the web version of the article.)

Our calculations revealed that the tips of the loops I and II are curved to the "convex side" with CA shift of 3.0 Å for Ser8, 3.5 Å for Ser9, 5.9 Å for His31 and 4.1 Å for Arg32 (Fig. 4), with the overall structure CA rmsd value of 1.45. Interestingly, the tip of the loop II was found by ^{1}H NMR to be the most flexible in free homologous α-toxin (Guenneugues et al., 1997). In addition, the flexibility of loop II was manifested as a change of chemical shifts for Ile35 observed upon NTII binding to Torpedo nAChRs membranes (Krabben et al., 2004).

Application of AMBER'99 and GROMOS'87 MD calculations proved the validity of the model for the chosen docking solution. During the MD calculation, all elements of secondary structure were well preserved and most of the contacts between the NTII and nAChR residues found by docking simulation were generally retained during MD operations (compare Tables 1 and 2). In the case of AMBER'99 (to a less extent for GROMOS'87 force field) simulation, the toxin molecule squeezed even a bit further between the subunits. The highly conserved and structurally stable cystine-rich core of the toxin, which was initially more distant from the receptor's subunits, approached the γ-subunit (it took 15–25 ps), resulting in a decrease by ∼10° of the angle between the principal molecular axes of the toxin and receptor. GROMOS'87 study did not reveal any changes in angles but showed that the distant parts of the toxin had shrunk in the direction of the pocket. In both cases MD calculations generated the additional contacts of those parts of NTII (His4 and Gln7 in loop I, Lys25, Trp27, Arg38 in loop II, Lys44, Asn50, Asn52 and Asn61 in loop III, see Table 2) which could be characterized as important, but not critical

for interaction with the receptor. Similar conclusions were drawn from mutagenesis studies of α-toxins from *N. nigricollis* (Pillet et al., 1993; Tremeau et al., 1995) and *Naja mossambica mossambica* (Ackermann and Taylor, 1996; Ackermann et al., 1998; Osaka et al., 2000). It is worth to mention that Arg36 of neurotoxin I from *N. mossambica mossambica* (homologous to Arg38 of NTII) failed to form an identified contact with the complementary side of the α–γ interface in pair-wise experiments, probably because of only a small number of tested mutant receptors (Ackermann et al., 1998). In the frames of our model, Arg38 forms an ionic pair with the γ-subunit Asp30 that correlates with the energy profit found for the contact of Arg36 from neurotoxin I with nAChR. In addition, experimentally measured distances (Michalet et al., 2000) between the tips of loops I and II of the α-toxin *N. nigricollis* bound to α–γ site of the *T. marmorata* nAChR, and Cys192–Cys193 bridge of the α-subunit are close to those obtained by our modeling (11.5 Å and 15.5 Å versus 10.5 Å and 15.0–18.9 Å).

Docking simulation revealed five contacts of particular interest between residues of the receptor and NTII, which seem to determine mainly their specific interaction (Table 1). The kinetics of changing of distances characterizing these contacts is presented in Fig. 5. Two of these toxin residues, Arg32 and Lys46, were found to be the most critical for activity of a short neurotoxin (Ackermann and Taylor, 1996; Kreienkamp et al., 1992; Tremeau et al., 1995; Tsetlin et al., 1982). On the other hand, several receptor residues (αTrp149, γTrp55, γGln57 and γTyr117), shown by mutagenesis to be essential for binding of neurotoxin I from *N. mossambica mossambica* (Ackermann and Taylor, 1996; Osaka et al., 2000), form strong contacts with NTII in our model (Tables 1 and 2). In addition, in our model we also see the toxin interaction with several nAChR residues (αTyr93, αTrp149, αTyr190, αTyr198 and γTrp55), which are indispensable for agonist binding (Galzi et al., 1991; Sullivan et al., 2002).

However, several contacts deduced from pair-wise mutations are absent in the model. For example, there is no interaction with αPro197. Apparently, this residue is playing an important role in the maintenance of the C-loop structure, and its mutation thus should affect the toxin binding. Our results support the significance of the method of pair-wise mutations, but also show the need of cautious interpretation of experimental data.

Qualitative information about the nAChR binding sites from earlier spectroscopic and photolabeling studies on the fluorescence, spin-labeled and photoactivatable derivatives of NTII can be rationalized in the frames of our model.

Because the side chains of the neighboring Lys25 and Lys26 are oppositely directed relative to plane of loop II (Fig. 4) and different labels (photoactivalable, spin, fluorescence) grafted on them made cross-links or "felt" the receptor surface, it was postulated that the toxin loop II should penetrate into nAChR (Tsetlin et al., 1982; Hucho et al., 1996).

It was previously shown that fluorescence spectra of NTII having dansyl (DNS) labels at Lys46, Lys25 and Lys26 undergo blue shift when respective derivatives are bound to the receptor (Tsetlin et al., 1982). The proximity of a tryptophan residue of the *Torpedo* nAChR to Lys46 position was suggested, as Lys46-DNS derivate demonstrated enhanced fluorescence at λ_{excit} 298 nm in the receptor complex. In our model, there is γTrp170 at the α–γ interface just near the Lys46 (Table 2). A hydrophobic surrounding is found for Lys26 and Lys25. Since Leu1 and Lys15 were not found to interact with the receptor in our model, the absence of large differences between fluorescence of free and bound Leu1 and Lys15 NTII DNS derivatives is not surprising.

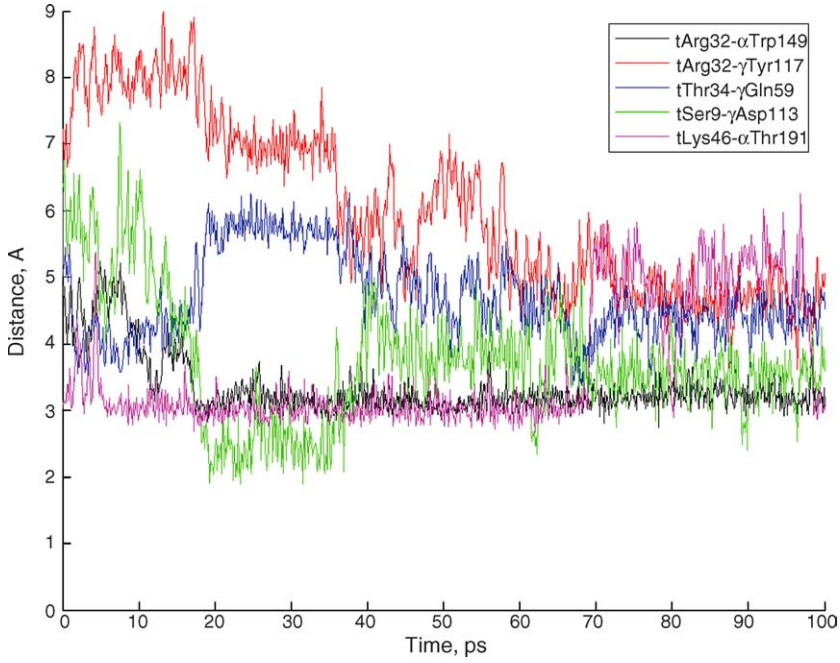

Fig. 5. Kinetics of the distances between functional groups of contacting residues (3 ps of preliminary relaxation are not shown) in AMBER'99 force field. It is seen that according to AMBER'99 the contacts mentioned in the legend are roughly within a radius of 5 Å.

For spin-labeled NTII derivatives it was found that the labels on Lys25, Lys26 and His31 became less flexible when the toxin was bound to the receptor (Tsetlin et al., 1982). This correlates with the contacts identified by the model: His31 is entering the binding pocket, Lys25 interacts with the complementary side, and Lys26 is hindered by side chains of loops I and III as well as by the tip of the receptor C-loop (Tables 1 and 2; Fig. 4). Interestingly, the accessibility of the labels to the paramagnetic probes diminishes for Lys26 and Lys46 and dramatically decreases for His31 when the toxin is bound to the receptor (Tsetlin et al., 1982). The model is also in accord with these data, since by docking and MD the His31 was found to be deeply inserted into the binding pocket and Lys46 to interact with the F-loop of the complementary side and the C-loop of the principal. For label on Lys26, the proximity to a negatively charged or sulfur-containing group of the receptor was suggested (Tsetlin et al., 1982), and the closeness to the αCys192–αCys193 disulfide was shown by the model.

The results of numerous photolabeling experiments can find explanation in the frames of our model. For example, it is obvious why the two α-subunits are the predominant cross-linking sites for the *p*-azidobenzoyl group at the Lys46, while for the same label at Lys26 the major cross-links are with the δ- and γ-subunits (Kreienkamp et al., 1992). The cross-linking to the δ-subunit with nitrodiazirine labels at positions 25 and 44 is also in good accordance with the model (Utkin et al., 1995).

The distance from the toxin center to the outer membrane surface (∼25 Å) estimated from the δ-subunit cross-link with the Lys25 azidosalicylamidoethyl-1,3-dithiopropyl (ASED) derivative of NTII (Machold et al., 1995a) is in accord with that proposed by our model. However, the contact as such with δAla268 is not easy to realize in the frames of the model. The same concerns labeling of the β-subunit by Lys15 derivatives of NTII bearing ASED or benzoylbenzoyl photolabels (Machold et al., 1995b; Kasheverov et al., 1999). The reason might be in changing of the correct positioning of NTII carrying bulky label as compared with binding of unmodified toxin. On the other hand, cross-linking to the neighboring receptor molecules in tightly packed membranes (Unwin, 2005) cannot be excluded for the toxins derivatives with photolabels attached via long spacer arms. Indeed, it was shown that perturbation of the membrane structure with temperature or non-ionic detergents might affect toxin binding at equilibrium and the photoinduced cross-links (Saez-Briones et al., 1999).

3.4. A comparison of the nAChR and AChBP complexes with short α-neurotoxin, long α-neurotoxin and α-conotoxin

The proposed model shows that the C-loop outward shift is critical for short α-neurotoxin NTII binding to the nAChR. The same was found by X-ray analysis for the complexes of AChBPs with α-cobratoxin from *Naja kaouthia* (Bourne et al., 2005) or with α-conotoxin PnIA analog (Celie et al., 2005). The spatial disposition of the C-loop disulfide Cys192–Cys193 in complexes with antagonists (Bourne et al., 2005; Celie et al., 2005) and agonists (Celie et al., 2004, 1UW6, 1UV6) is changed as compared to its position in the intact nAChR (Unwin, 2005, see 2BG9 structure). The C-loop of the α-subunit did not virtually change its shifted position in complex even after 100 ps MD simulations, just the winding of the loop (residues 194–198) redistributed along the primary structure. This fragment has no direct contacts with NTII, and preserves relative flexibility limited by αCys192, αCys193 and αTyr198 involvement in the toxin-receptor interaction. Similar fluctuations were previously suggested for AChBP–agonist complexes on the basis of fluorescence studies and MD simulations (Gao et al., 2005). Moreover, a non-restricted mobility of the α-subunit C-loop in the resting state of the receptor was suggested (Bourne et al., 2005). Our model provides an additional support to this hypothesis because formation of even unstable complex of the toxin with receptor having a closed C-loop was not possible by docking simulations.

In contrast, docking of the NMR structures of NTII was successful if the C-loop was drawn aside from the receptor's body. Subsequent MD simulations resulted in some local conformational changes in the toxin. However, for initial entry into the receptor-binding pocket the toxin should "seize the moment" when the C-loop is going out. When the C-loop protrudes from the receptor surface, the toxin inserts its loop II, with Arg32 emulating the positive charge of the agonist into the ligand-binding pocket. Then the toxin loops I and III interact by their tips with the receptor residues. This should be a very fast process that is why the toxins maintain a very rigid structure ideally adapted for pocket entering. Interestingly, the kinetics of the binding of short neurotoxins to the receptor was experimentally found to be very fast (Chicheportiche et al., 1975; Endo et al., 1986). Thus, diverse perturbations of the toxin structure, such as an introduction of a bulky label at Lys25, which might alter the angle of entry, or mutation of Lys26 whose salt bridge with Glu37 maintains the stability of the loop, may influence the kinetics and affinity of the toxin for the receptor.

The turn of the α-subunit of the receptor, similar to that postulated for agonist binding (Unwin et al., 2002; Unwin, 2005), was required to accommodate a short α-neurotoxin in our model (Fig. 2). A slight rigid-body rotation of protomers was also detected for AChBP in complex with α-conotoxin (Celie et al., 2005). The conformational changes detected by MD simulations are virtually equal to those required for the formation of the final stable complex. The number of contacts considerably increases (compare Tables 1 and 2) and the interaction surface becomes larger, especially on the complementary side (Fig. 6). Just 15–25 ps is enough for the rearrangement of the toxin–receptor complex. This position of the toxin is stable, at least for 100 ps, as was found by MD dynamics.

The interaction of α-cobratoxin from *N. kaouthia* with AChBP was shown to evoke a downstream shift of the F-loop on the complementary side of the pocket (Bourne et al., 2005). This toxin introduces the tip of its loop II into the pocket from the so-called "small cavity" and from bottom of the C-loop (Fig. 7c). According to our model, a short α-neurotoxin interacts with the receptor in a different mode entering the pocket from the top-right (looking from the outside of the subunit pore) of the C-loop from the "big cavity" (Fig. 7b). This way of forming the complex is more similar to that of the AChBP–conotoxin (Fig. 7a). Therefore, there are clear differences in certain details of bind-

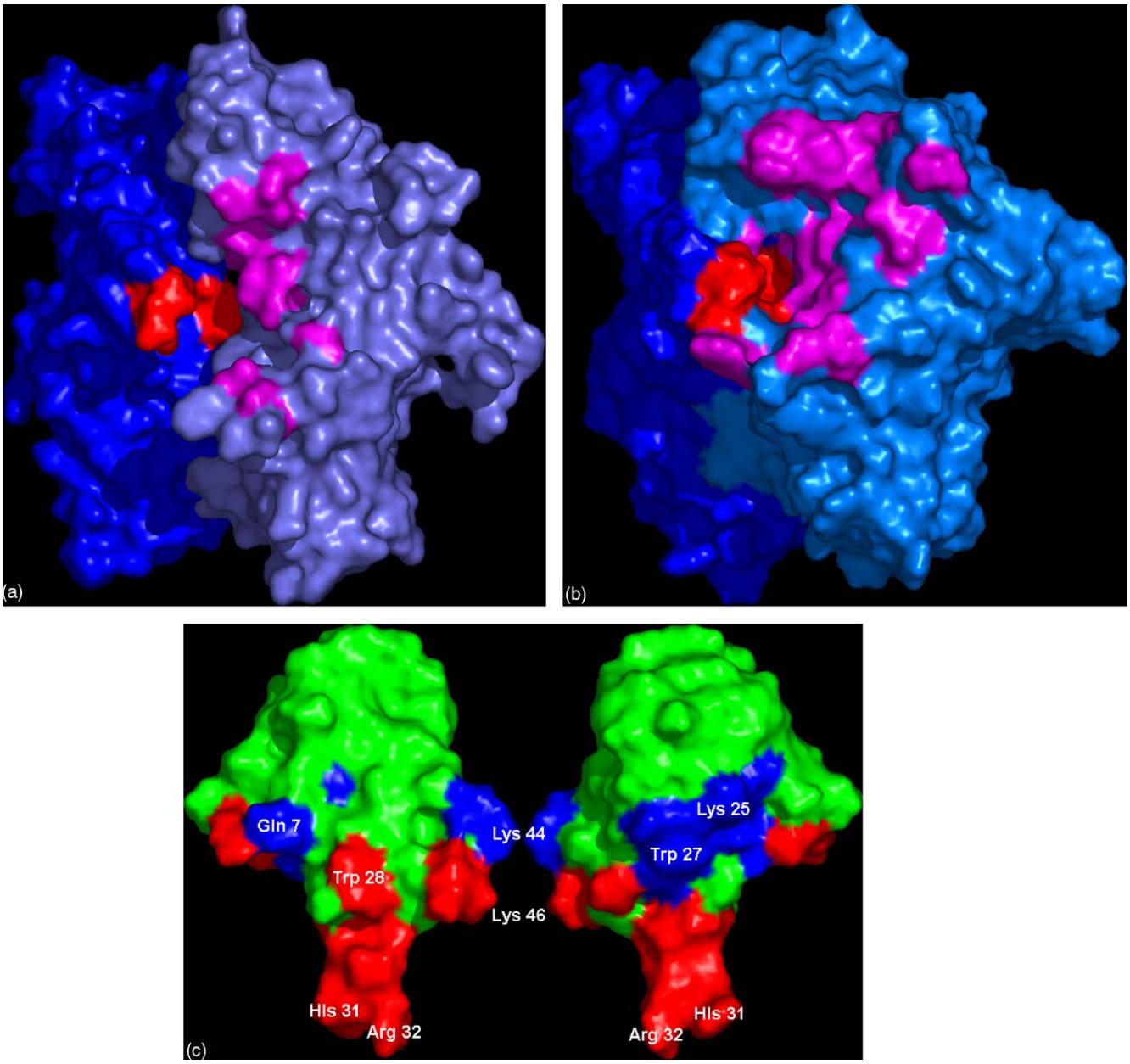

Fig. 6. Surface image of binding pocket on the nAChR α–γ interface according to docking simulations (a) and after MD calculations (b). Designation by color: blue, principal side; red, residues interacting with the toxin; marine, complementary side; magenta, residues interacting with the toxin. Rearrangement of the binding site can be seen. (c) Surface image of NTII in the binding pocket from toxin "concave side" (left) and toxin "convex side" (right). Some residues found to be involved in interaction both by the docking simulation and MD are in red, only by MD, in blue. (For interpretation of the references to color in this figure legend, the reader is referred to the web version of the article.)

ing between short and long α-neurotoxins, belonging to the same family of the three-finger snake venom proteins.

On the other hand, a general similarity of their binding modes is also evident. As follows from the biochemical, molecular biology and electrophysiology data supported by X-ray (Celie et al., 2004), MD and fluorescence spectroscopy (Gao et al., 2005), as well as by cryo-electron microscopy data (Unwin, 2005), agonist binding evokes the formation of the "aromatic box" built of αTrp149, αTyr93, αTyr190, αTyr198 and γTrp55 residues (*T. californica* α–γ interface numeration) around the positive charge of a ligand. Both α-cobratoxin and NTII have positive charges at the tip of loop II (Arg33 and Arg32, respectively) that partially mimic the charge of the agonist nitrogen. However, neither long, nor short α-neurotoxins permits the assembly of the box, breaking it with aromatic moieties of Phe29 and His31, respectively (Fig. 8).

Paradoxically, α-conotoxin sterically emulates nicotine by its double proline sequence Pro6Pro7. The aromatic residues of the nAChR are oriented roughly in the same way as in the complex with an agonist (Celie et al., 2004, 2005). Moreover, while α-conotoxin [A10L]PnIA is an antagonist of the neuronal α7 nAChR, with the same receptor bearing a Leu247Thr mutation

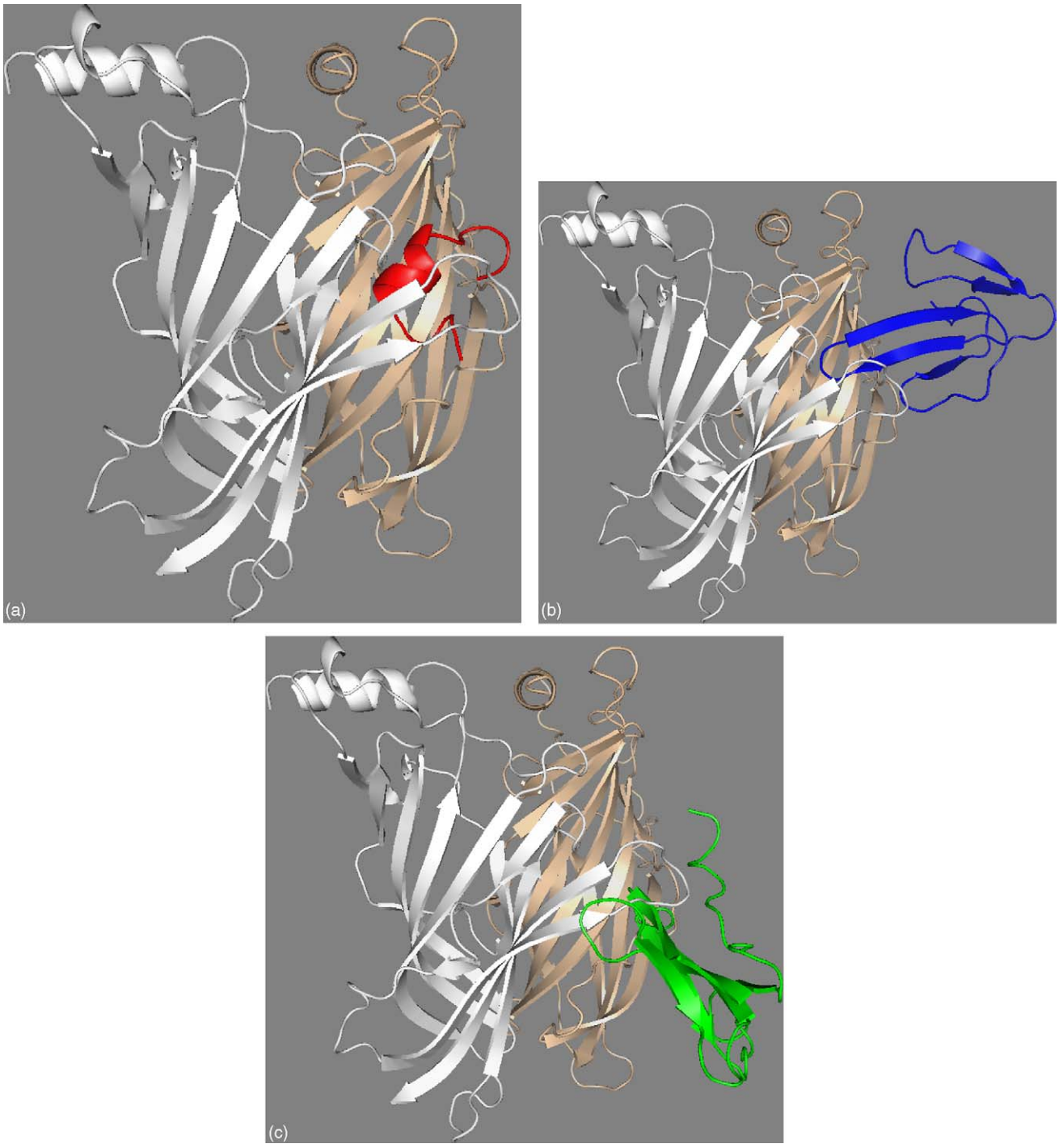

Fig. 7. Comparison of the positions of α-conotoxin PnIA analog (a), short α-neurotoxin NTII (b), long α-neurotoxin α-bungarotoxin from *Bungarus multicinctus* (c) in the ligand-binding site represented on α–γ interface of *Torpedo californica* nAChR. The position of conotoxin was taken from 2BR8. The position of NTII was obtained by fitting of described model structure. The position of the α-bungarotoxin was determined by 1L4W structure fitting to 2BR8 and fast MD simulations (10 ps) in AMBER'99 force field and was similar to that found for α-cobratoxin (Bourne et al., 2005). Protomers colored in white and wheat; ligands in red, blue and green, respectively. (For interpretation of the references to color in this figure legend, the reader is referred to the web version of the article.)

in the transmembrane segment this α-conotoxin at relatively high concentrations plays the role of an agonist (Hogg et al., 2003).

Some local conformational changes in the binding pocket induced by agonist binding should lead to a more global rearrangement of the receptor molecule resulting in the channel opening. The snake toxins are blocking this rearrangement, not allowing a correct assembly of the binding pocket and occupying the place of agonist. An α-conotoxin, also placed in the agonist-binding pocket, still permits the proper rearrangement of the

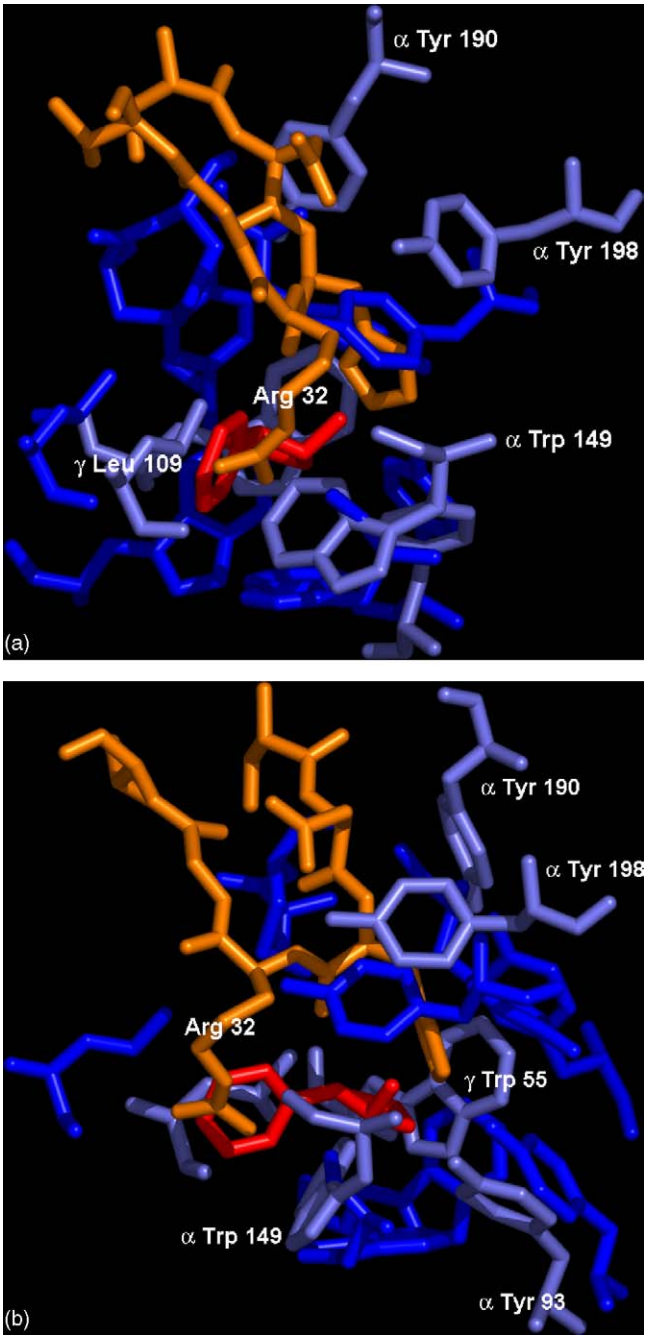

Fig. 8. Fit of the AChBP–nicotine complex X-ray structure (1UW6) and NTII–nAChR α–γ interface complex model. View from the "big cavity" (a) and principal side B-loop (b). Differences in position of aromatic residues of the receptor-binding pocket are visible. Designation by color: agonist binding pocket if nicotine bound to AChBP in blue, the same pocket of α–γ interface of nAChR if toxin bound in slate, nicotine in red, loop II tip in orange. Some residues of nAChR and Arg32 of NTII are shown. (For interpretation of the references to color in this figure legend, the reader is referred to the web version of the article.)

pocket, but the channel remains closed. Thus, formation of the "aromatic" box is an essential but not the sole conformational change that leads to the opening of the receptor channel. In any case, short and long α-neurotoxins have many common features in their receptor binding modes, which differ considerably from that of α-conotoxins.

4. Conclusion

A first model for the interaction of short α-neurotoxin with the *T. californica* nAChR has been built taking into account the relevant three-dimensional structures. It is shown to be in accord with numerous experimental data proving the validity both of this model and of the employed methodology. Thus, the computational approach may be used to rationalize the existing experimental data and to design new antagonists and agonists of diverse nAChRs for pharmacological purposes.

Acknowledgements

The authors are grateful to Profs. A.B. Smit, T. Sixma (Amsterdam) and V.T. Ivanov (Moscow) for fruitful discussions.

The work was supported in part by RFBR grant 05-04-48932 and NOW-RBRF grant (Prof. A.B. Smit (Amsterdam) and Prof. V.I. Tsetlin (Moscow).

References

Ackermann, E.J., Taylor, P., 1996. Nonidentity of the alpha-neurotoxin binding sites on the nicotinic acetylcholine receptor revealed by modification in alpha-neurotoxin and receptor structures. Biochemistry 36, 12836–12844.

Ackermann, E.J., Ang, E.T.-H., Kanter, J.R., Tsigelny, I., Taylor, P., 1998. Identification of pairwise interactions in the neurotoxin–nicotinic acetylcholine receptor complex through double mutant cycles. J. Biol. Chem. 273, 10958–10964.

Arseniev, A.S., Utkin, Yu.N., Tsetlin, V.I., Ivanov, V.T., Bystrov, V.F., Ovchinnikov, Yu.A., 1981. ^{19}F NMR determination of intramolecular distances in spin and fluorine labeled proteins, neurotoxin II from *Naja naja oxiana*. FEBS Lett. 136, 269–274.

Blinov, N.O., Tsetlin, V.I., Utkin, Yu.N., 1982. Influence of acetylation of lysines of the neurotoxin II from *Naja naja oxiana* on neurotoxic activity. Bioorgan. Khim. 8, 165–168.

Bourne, Y., Talley, T.T., Hansen, S.B., Taylor, P., Marchot, P., 2005. Crystal structure of Cbtx–AChBP complex reveals essential interactions between snake alpha-neurotoxins and nicotinic receptors. EMBO J. 24 (8), 1512–1522.

Brejc, K., van Dijk, W.J., Klaassen, R.V., Schuurmans, M., van Der Oost, J., Smit, A.B., Sixma, T.K., 2001. Crystal structure of an ACh-binding protein reveals the ligand-binding domain of nicotinic receptors. Nature 411 (6835), 269–276.

Burkert, U., Allinger, N.L., 1982. Molecular Mechanics. ACS Monograph 177. American Chemical Society, Washington, DC.

Celie, P.H., Kasheverov, I.E., Mordvintsev, D.Y., Hogg, R.C., van Nierop, P., van Elk, R., van Rossum-Fikkert, S.E., Zhmak, M.N., Bertrand, D., Tsetlin, V., Sixma, T.K., Smit, A.B., 2005. Crystal structure of nicotinic acetylcholine receptor homolog AChBP in complex with an alpha-conotoxin PnIA variant. Nat. Struct. Mol. Biol. 12 (7), 582–588.

Celie, P.H., van Rossum-Fikkert, S.E., van Dijk, W.J., Brejc, K., Smit, A.B., Sixma, T.K., 2004. Nicotine and carbamylcholine binding to nicotinic acetylcholine receptors as studied in AChBP crystal structures. Neuron 41 (6), 907–914.

Changeux, J.-P., Edelstein, S.J., 1998. Allosteric recepors after 30 years. Neuron 21, 959–980.

Chicheportiche, R., Rochat, C., Sampiere, F., Lazdunski, M., 1972. Structure–function relationship of neurotoxins isolated from *Naja haje venom*. Physico-chemical properties and identification of the active site. Biochemistry 11, 1681–1691.

Chicheportiche, R., Vincent, J.P., Kopeyan, C., Schweitz, H., Lazdunski, M., 1975. Structure–function relationship in the binding of snake neurotoxins to the *Torpedo* membrane receptor. Biochemistry 14, 2081–2091.

Endo, T., Nakanishi, M., Furukawa, S., Joubert, F.J., Tamiya, N., Hayashi, K., 1986. Stopped-flow fluorescence studies on binding kinetics of neurotoxins with acetylcholine receptor. Biochemistry 25 (2), 395–404.

Fruchart-Gaillard, C., Gilquin, B., Antil-Delbeke, S., Le Novere, N., Tamiya, T., Corringer, P.J., Changeux, J.P., Menez, A., Servent, D., 2002. Experimentally based model of a complex between a snake toxin and the alpha 7 nicotinic receptor. PNAS 99 (5), 3216–3221.

Galzi, J.-L., Revah, F., Bessis, A., Changeux, J.-P., 1991. Functional architecture of the nicotinic acetylcholine receptor: from electric organ to brain. Annu. Rev. Pharmacol. 31, 37–72.

Gao, F., Bren, N., Burghardt, T.P., Hansen, S., Henchman, R.H., Taylor, P., McCammon, J.A., Sine, S.M., 2005. Agonist-mediated conformational changes in acetylcholine-binding protein revealed by simulation and intrinsic tryptophan fluorescence. J. Biol. Chem. 280 (9), 8443–8451.

Golo, V.L., Salnikov, V.N., Shaitan, K.V., 2004. Harmonic oscillators in the Nosé–Hoover environment. Phys. Rev. Evol. 70, 046130.

Golo, V.L., Shaitan, K.V., 2002. Dynamic attractor for the Berendsen thermostat and the slow dynamics of biomacromolecules. Biofizika 47, 61–617 (translation from Russian).

Golovanov, A.P., Lomize, A.L., Arseniev, A.S., Utkin, Y.N., Tsetlin, V.I., 1993. Two-dimensional ^{1}H-NMR study of the spatial structure of neurotoxin II from *Naja naja oxiana*. Eur. J. Biochem. 213 (3), 1213–1223.

Guenneugues, M., Pascal, Drevet, Suzanne, Pinkasfeld, Bernard, Gilquin, Andreĭ, Menez, Sophie, Zinn-Justin, 1997. Picosecond to hour time scale dynamics of a “three finger” toxin: correlation with its toxic and antigenic properties. Biochemistry 36, 16097–16108.

Gunsteren, W.F.van, Mark, A.E., 1992. On the interpretation of biochemical data by molecular dynamics computer simulation. Eur. J. Biochem. 204, 947–961.

Harel, M., Kasher, R., Nicolas, A., Guss, J.M., Balass, M., Fridkin, M., Smit, A.B., Brejc, K., Sixma, T.K., Katchalski-Katzir, E., Sussman, J.L., Fuchs, S., 2001. The binding site of acetylcholine receptor as visualized in the X-ray structure of a complex between alpha-bungarotoxin and a mimotope peptide. Neuron 32 (2), 265–275.

Hogg, R.C., Hopping, G., Alewood, P.F., Adams, D.J., Bertrand, D., 2003. Alpha-conotoxins PnIA and [A10L]PnIA stabilize different states of the alpha7-L247T nicotinic acetylcholine receptor. J. Biol. Chem. 278 (29), 26908–26914.

Hori, H., Tamiya, N., 1976. Preparation and activity of guanidinated or acetylated erabutoxins. Biochem. J. 153, 217–222.

Hucho, F., Tsetlin, V.I., Machold, J., 1996. The emerging three-dimensional structure of a receptor. The nicotinic acetylcholine receptor. Eur. J. Biochem. 239, 539–557.

Ivanov, V.T., Tsetlin, V.I., Karlsson, E., Arseniev, A.S., Utkin, Yu.N., Pashkov, V.S., Surin, A.M., Pluzhnikov, K.A., Bystrov, V.F., 1980. Spin and fluorescence labeled neurotoxin II. Conformational studies and interaction of the toxin with the acetylcholine receptor. In: Eaker, D., Wadstrom, T. (Eds.), Natural Toxins. Pergamon Press, Oxford, New York, pp. 523–530.

Kasheverov, I., Zhmak, M., Chivilyov, E., Saez-Brionez, P., Utkin, Yu., Hucho, F., Tsetlin, V.I., 1999. Benzophenone-type photoactivatable derivatives of α-neurotoxins and α-conotoxins in studies on *Torpedo* nicotinic acetylcholine receptor. J. Recept. Signal Transduct. Res. 19, 559–571.

Khechinashvili, N.N., Tsetlin, V.I., 1984. Calorimetric study of heat denaturation of toxins. Mol. Biol. (Mosk.) 18 (3), 786–791 (Russian).

Krabben, L., van Rossum, B.J., Castellani, F., Bocharov, E., Schulga, A.A., Arseniev, A.S., Weise, C., Hucho, F., Oschkinat, H., 2004. Towards structure determination of neurotoxin II bound to nicotinic acetylcholine receptor: a solid-state NMR approach. FEBS Lett. 564 (3), 319–324.

Kreienkamp, H.-J., Utkin, Yu.N., Weise, C., Machold, J., Tsetlin, V.I., Hucho, F., 1992. Investigation of ligand-binding sites of the acetylcholine receptor using photoactivatable derivatives of neurotoxin II from *Naja naja oxiana*. Biochemistry 31, 8239–8244.

Lemak, A.S., Balabaev, N.K., 1995. A comparison between collisional dynamics and Brownian dynamics. Mol. Simul. 15, 223–231.

Lemak, A.S., Balabaev, N.K., 1996. Molecular dynamics simulation of a polymer chain in solution by collisional dynamics method. J. Comp. Chem. 17, 1685–1695.

Machold, J., Utkin, Yu., Kirsch, D., Kaufmann, R., Tsetlin, V., Hucho, F., 1995a. Photolabeling reveals the proximity of the α-neurotoxin binding site to M2 helix of the ion channel in the nicotinic acetylcholine receptor. Proc. Natl. Acad. Sci. U.S.A. 92, 7282–7286.

Machold, J., Weise, C., Utkin, Y.N., Franke, P., Tsetlin, V.I., Hucho, F., 1995b. A new class of photoactivatable and cleavable derivatives of neurotoxin II from *Naja naja oxiana*. Synthesis, characterisation, and application for affinity labelling of the nicotinic acetylcholine receptor from *Torpedo californica*. Eur. J. Biochem. 228 (3), 947–954.

Michalet, S., Teixeira, F., Gilquin, B., Mourier, G., Servent, D., Drevet, P., Binderi, P., Tzartos, S., Menez, A., Kessler, P., 2000. Relative spatial position of a snake neurotoxin and the reduced disulfide bond alpha(Cys192–Cys193) at the alpha–gamma interface of the nicotinic acetylcholine receptor. J. Biol. Chem. 275 (33), 25608–25615.

Neubig, R.R., Cohen, J.B., 1979. Equilibrium binding of [3H]tubocurarine and [^{3}H]acetylcholine by *Torpedo* postsynaptic membranes: stoichiometry and ligand interactions. Biochemistry 18, 5464–5475.

Nirthanan, S., Gwee, M.C., 2004. Three-finger alpha-neurotoxins and the nicotinic acetylcholine receptor, 40 years on. J. Pharmacol. Sci. 94 (1), 1–17.

Osaka, H., Malany, S., Molles, B.E., Sine, S.M., Taylor, P., 2000. Pairwise electrostatic interactions between alpha-neurotoxins and gamma, delta and epsilon subunits of the nicotinic acetylcholine receptor. J. Biol. Chem. 275, 5478–5484.

Paas, Y., Cartaud, J., Recouvreur, M., Grailhe, R., Dufresne, V., Pebay-Peyroula, E., Landau, E.M., Changeux, J.-P., 2003. Electron microscopic evidence for nucleation and growth of 3D acetylcholine receptor microcrystals in structured lipid-detergent matrices. PNAS 100, 11309–11314.

Pillet, L., Tremeau, O., Ducancel, F., Drevet, P., Zinn-Justin, S., Pinkasfeld, S., Boulain, J.C., Menez, A., 1993. Genetic engineering of snake toxins. Role of invariant residues in the structural and functional properties of a curaremimetic toxin, as probed by site-directed mutagenesis. J. Biol. Chem. 268 (2), 909–916.

Saez-Briones, P., Krauss, M., Dreger, M., Herrmann, A., Tsetlin, V.I., Hucho, F., 1999. How do acetylcholine receptor ligands reach their binding sites? Eur. J. Biochem. 265 (3), 902–910.

Samson, A., Scherf, T., Eisenstein, M., Chill, J., Anglister, J., 2002. The mechanism for acetylcholine receptor inhibition by alpha-neurotoxins and species-specific resistance to alpha-bungarotoxin revealed by NMR. Neuron 35 (2), 319–332.

Servent, D., Menez, A., 2001. Snake neurotoxins that interact with nicotinic acetylcholine receptors. In: Massaro, E.J. (Ed.), Handbook of Neurotoxicology, vol. 1. Humana, Totowa, NJ, pp. 385–425.

Stroud, R.M., McCarthy, M.P., Shuster, M., 1990. Nicotinic acetylcholine receptor superfamily of ligand-gated ion channels. Biochemistry 29, 11009–11023.

Sullivan, D., Chiara, D.C., Cohen, J.B., 2002. Mapping the agonist binding site of the nicotinic acetylcholine receptor by cysteine scanning mutagenesis: antagonist footprint and secondary structure prediction. Mol. Pharmacol. 61 (2), 463–472.

Teixeira-Clerc, F., Menez, A., Kessler, P., 2002. How do short neurotoxins bind to a muscular-type nicotinic acetylcholine receptor? J. Biol. Chem. 277, 25741–25747.

Timofeev, V.P., Tsetlin, V.I., 1983. Analysis of mobility of protein side chains by spin label technique. Biophys. Struct. Mech. 10, 93–108.

Tremeau, O., Lemaire, C., Drevet, P., Pinkasfeld, S., Ducance, l.F., Boulain, J.C., Menez, A., 1995. Genetic engineering of snake toxins. The functional site of Erabutoxin a, as delineated by site-directed mutagenesis, includes variant residues. J. Biol. Chem. 270 (16), 9362–9369.

Tsetlin, V.I., 1999. Snake venom alpha-neurotoxins and other ‘three-finger’ proteins. Eur. J. Biochem. 264 (2), 281–286.

Tsetlin, V.I., Hucho, F., 2004. Snake and snail toxins acting on nicotinic acetylcholine receptors: fundamental aspects and medical applications. FEBS Lett. 557, 9–13.

Tsetlin, V.I., Karlsson, E., Arseniev, A.S., Utkin, Yu.N., Surin, A.M., Pashkov, V.S., Pluzhnikov, K.A., Ivanov, V.T., Bystrov, V.F., Ovchinnikov, Yu.A., 1979a. EPR and fluorescence study of interaction of *Naja naja oxiana* neurotoxin II and its derivatives with acetylcholine receptor protein from *Torpedo marmorata*. FEBS Lett. 106, 47–52.

Tsetlin, V.I., Arseniev, A.S., Utkin, Yu.N., Gurevich, A.Z., Senyavina, L.B., Bystrov, V.F., Ivanov, V.T., Ovchinnikov, Yu.A., 1979b. Conformational studies of neurotoxin II from *Naja naja oxiana*. Selective *N*-acylation, circular dichroism and NMR study of acylation products. Eur. J. Biochem. 94, 337–346.

Tsetlin, V.I., Karlsson, E., Utkin, Yu.N., Pluzhnikov, K.A., Arseniev, A.S., Surin, A.M., Kondakov, V.I., Bystrov, V.F., Ovchinnikov, Yu.A., 1982. Interacting surfaces of neurotoxins and acetylcholine receptor. Toxicon 20, 83–93.

Unwin, N., Miyazawa, A., Li, J., Fujiyoshi, Y., 2002. Activation of the nicotinic acetylcholine receptor involves a switch in conformation of the alpha subunits. J. Mol. Biol. 319 (5), 1165–1176.

Unwin, N., 2005. Refined structure of the nicotinic acetylcholine receptor at 4 A° resolution. J. Mol. Biol. 346, 967–989.

Utkin, Y.N., Kobayashi, Y., Hucho, F., Tsetlin, V.I., 1994. Relationship between the binding sites for an alpha-conotoxin and snake venom neurotoxins in the nicotinic acetylcholine receptor from *Torpedo californica*. Toxicon 32 (9), 1153–1157.

Utkin, Y.N., Hatanaka, Y., Franke, P., Machold, J., Hucho, F., Tsetlin, V.I., 1995. Synthesis of nitrodiazirinyl derivatives of neurotoxin II from *Naja naja oxiana* and their interaction with the *Torpedo californica* nicotinic acetylcholine receptor. J. Protein Chem. 4, 197–203.

Wang, J.M., Cieplak, P., Kollman, P.A., 2000. How well does a restrained electrostatic potential (RESP) model perform in calculating conformational energies of organic and biological molecules? J. Comp. Chem. 21, 1049–1074.

Yang, C.C., 1974. Chemistry and evolution of toxins in snake venoms. Toxicon 12, 1–43.